(1958).

[2]Y. Toyozawa, Progr. Theoret. Phys. (Kyoto) 27, 89 (1962).

[3]Y. Toyozawa, J. Phys. Chem. Solids 25, 59 (1964).

[4]J. E. Eby, K. J. Teegarden, and D. B. Dutton, Phys. Rev. 116, 1099 (1959).

[5]H. R. Philipp and H. Ehrenreich, Phys. Rev. 131, 2016 (1963).

[6]K. Teegarden and G. Baldini, Phys. Rev. 155, 896 (1967).

[7]G. Baldini, A. Bosacchi, and B. Bosacchi, Phys. Rev. Letters 23, 846 (1969).

[8]J. J. Hopfield, J. M. Worlock, and K. Park, Phys. Rev. Letters 11, 414 (1963).

[9]J. J. Hopfield and J. M. Worlock, Phys. Rev. 137, A1455 (1965).

[10]M. L. Cohen, P. J. Lin, D. M. Roessler, and W. C. Walker, Phys. Rev. 155, 992 (1967).

[11]Y. Onodera and M. Okazaki, J. Phys. Soc. Japan 21, 2229 (1966).

[12]Y. Onodera and Y. Toyozawa, J. Phys. Soc. Japan 22, 833 (1967).

[13]W. Y. Liang and A. D. Yoffe, Phys. Rev. Letters 20, 59 (1968).

[14]W. C. Walker, D. M. Roessler, and E. Loh, Phys. Rev. Letters 20, 847 (1968).

[15]Y. Toyozawa and J. Hermanson, Phys. Rev. Letters 21, 1637 (1968).

[16]H. Fröhlich, Advan. Phys. 3, 325 (1954).

[17]W. P. Dumke, Phys. Rev. 108, 1419 (1957).

[18]D. G. Thomas, J. J. Hopfield, and M. Power, Phys. Rev. 119, 570 (1960).

[19]B. Segall, Phys. Rev. 150, 734 (1966).

[20]B. Segall and G. D. Mahan, Phys. Rev. 171, 935 (1968).

[21]R. G. Stafford, Phys. Rev. B 3, 2729 (1971).

[22]G. D. Mahan, Phys. Rev. 170, 825 (1968).

[23]References cited in Ref. 22.

[24]R. J. Elliott, Phys. Rev. 108, 1384 (1957).

[25]K. Park and R. G. Stafford, Phys. Rev. Letters 22, 1426 (1969).

[26]J. Ramamurti and K. Teegarden, Phys. Rev. 145, 698 (1966).

[27]F. Fischer and R. Hilsch, Nachr. Akad. Wiss. Göttingen, II Math.-Physik. Kl. 8, 241 (1959).

[28]J. W. Hodby, J. A. Borders, and F. C. Brown, Phys. Rev. Letters 19, 952 (1967).

[29]C. Kittel, Quantum Theory of Solids (Wiley, New York, 1967).

[30]R. G. Stafford and K. Park, Phys. Rev. Letters 25, 1652 (1970).

[31]Note the absorption constant in Ref. 30 should be a factor of 4 smaller.

[32]R. J. Elliott, Phys. Rev. 124, 340 (1961).

[33]J. P. Dahl and A. C. Switendick, J. Phys. Chem. Solids 27, 931 (1966).

Phonon Structure of Impurity-Related Optical Spectra in Insulators[*]

M. Mostoller, B. N. Ganguly, and R. F. Wood

Solid State Division, Oak Ridge National Laboratory, Oak Ridge, Tennessee 37830

(Received 14 January 1971)

The theory of optical processes associated with point imperfections in insulating crystals is briefly reviewed and a practical efficient computational procedure is developed for the detailed application of the theory to systems whose spectra exhibit marked vibronic structure. This procedure includes the following features: (a) an iterative scheme for extracting the effective one-phonon density of states from experimental data; (b) the convolution of the one-phonon spectrum to find the contributions of those n-phonon processes which yield discernible vibronic structure and the use of moment analysis for higher n-phonon processes; (c) inclusion of the lowest-order effects of quadratic coupling on the temperature dependence of the zero-phonon line's half-width and peak position; (d) a simple transformation between phonon operators in the ground and excited electronic states of the impurity which breaks the mirror symmetry between the absorption and emission spectra characteristic of the strict linear-coupling approximation. The absorption spectrum of the N_1 color center in NaCl, which exhibits a great deal of phonon structure, is used to illustrate certain aspects of the calculations. Good agreement between theory and experiment is obtained for this example.

I. INTRODUCTION

The modifications of the electronic and vibrational properties of crystals produced by the introduction of point imperfections[1] have been investigated extensively in recent years. A particularly large amount of work has been devoted to the study of the optical absorption and emission spectra of defects and impurities in insulators, which display great variety ranging from smooth broad bands with little or no vibronic structure to spectra in which only sharp structure is observed. Although the theory of these optical processes is well understood by now, the calculations involved in its detailed application can become quite complicated. In spite of this, it would seem that the great wealth of information about the interacting electron-phonon system which is inherent in the theory warrants

considerable calculational effort. In this paper, we report on various aspects of our efforts to develop an efficient computational scheme which we believe can be applied to systems whose spectra exhibit a wide range of vibronic structure.

We have found it most convenient to follow the formulation of the theory presented by Lax[2] in 1952 and by McCumber[3] in a series of papers dating from 1964. Lax's work, which followed (chronologically) the work of Huang and Rhys,[4] Pekar,[5] and Williams,[6] does not explicitly discuss the zero-phonon line and other vibronic structure. This is not an inherent shortcoming of Lax's approach but merely reflects the fact that zero-phonon lines and vibronic structure had not been observed, or at least not widely studied experimentally, for defect systems at that time. Of the many papers which followed this earlier work, we would like to mention a few which we have found quite helpful, e.g., those of O'Rourke,[7] Keil,[8] and Markham,[9] and of the Russian authors such as Perlin,[10] Krivoglaz,[11] and Trifonov.[12] A summary of much of this work is contained in an article by Maradudin.[13] A review of both the experimental work and earlier applications of the theory to the class of defects (color centers) from which we shall later choose an illustrative example has been given by Fitchen.[14] From the foregoing it should be clear that very little will be said here about the semiclassical approach (Ref. 2) in which a model based on one or two configuration coordinates often suffices to give remarkably good agreement with smooth broad-band spectra. However, the connection between various quantities appearing in the two approaches is briefly sketched in Appendix A.

There are a few general remarks we would like to make about our work before beginning a more detailed account. From the calculations we have performed, we feel that it should be possible to obtain excellent agreement between theoretical and experimental absorption or emission curves for most cases in which the linear-coupling approximation is reasonably good. That is to say, the calculations required by the theory in this approximation can be carried out with great accuracy in a very short time on the present generation of electronic computers. A second remark has to do with the inclusion of quadratic coupling. Without quadratic coupling neither the width nor the position of the zero-phonon line would be temperature dependent, and the emission and absorption curves would be exact mirror images of one another about the zero-phonon line. These features are seldom if ever exactly observed in real crystals. We have therefore sought to include quadratic-coupling effects at a level of approximation which will provide for at least qualitative agreement with experimental data and yet allow the calculations to be carried

out in a reasonable length of time. We believe that these approximations will, in fact, be quantitatively sufficient for many impurities and color centers.

In Sec. II we give a brief review of the theory and describe a few developments which we have found useful in applications. In Secs. III and IV some of the computational details are explained and calculations on the N_1 center in NaCl are given as an example. In Sec. V, several features of our results are discussed and a number of conclusions drawn.

II. REVIEW AND DEVELOPMENT OF THEORY

A. Formulation of the Problem and Basic Assumptions

We consider the optical absorption and emission spectra arising from electronic transitions between the ground state and a singlet[15] excited state of an interacting defect-lattice system, making the following approximations:

(i) There is no coupling between the two electronic states via the electron-phonon interaction (the adiabatic approximation). The effective Hamiltonian for the system can then be written as

$$H = H_a C_a^\dagger C_a + H_b C_b^\dagger C_b , \qquad (1)$$

where the C's are the usual electron creation and destruction operators, and H_a and H_b are the ground- and excited-state phonon Hamiltonians, respectively, which, however, also contain the electronic energies at the equilibrium positions of the nuclei.

(ii) The electronic dipole moment matrix element for the transition does not depend on the ionic positions (the Condon approximation). This is expected to be a good approximation in many instances, but care must be exercised in its use since exceptional cases are known.

(iii) The phonons reach internal equilibrium in times short with respect to the radiative transition times, so that the phonon ensemble can be characterized by a definite temperature T.

With these approximations, the absorption cross section $\sigma_{ab}(\omega)$ and the spontaneous emission probability $W_{ba}(\omega)$ take the form[2,16]

$$\sigma_{ab}(\omega) = K_{\text{abs}} |M_{ab}|^2 \omega G(ab; \omega) , \qquad (2)$$

$$W_{ba}(\omega) = K_{\text{em}} |M_{ab}|^2 \omega^3 G(ba; \omega) . \qquad (3)$$

Here ω is the photon frequency, M_{ab} is the electronic dipole moment matrix element, and K_{abs} and K_{em} are quantities involving the effective field ratio and the dielectric constant which will be assumed independent of ω. With the Condon approximation, the spectral functions $G(ab; \omega)$ and $G(ba; \omega)$ are Fourier transforms of the square of overlap integrals between phonon wave functions in the ground and excited electronic states, averaged over the

appropriate initial-state phonon ensemble and summed over final states. In terms of the ground- and excited-state phonon Hamiltonians, the expression for the absorption function $G(ab;\omega)$ reduces to[2,13]

$$G(ab;\omega) = \int_{-\infty}^{\infty} dt\, e^{i\omega t} G(ab;t)$$

$$= \int_{-\infty}^{\infty} dt\, e^{i\omega t} \langle e^{iH_a t/\hbar} e^{-iH_b t/\hbar} \rangle_a , \quad (4)$$

where $\langle O \rangle_a$ denotes the average of a (phonon) operator O over the ground-state phonon ensemble, i. e.,

$$\langle O \rangle_a = \mathrm{Tr}\, e^{-\beta H_a} O / \mathrm{Tr}\, e^{-\beta H_a} .$$

In the emission function $G(ba;\omega)$, H_b and H_a are interchanged, the sign of the time is reversed, and the average is performed over the excited-state phonon ensemble.

Harmonic ground- and excited-state phonon Hamiltonians are assumed which, with different equilibrium ionic positions and force constants, may differ by terms of first and second order in the phonon amplitudes (linear and quadratic coupling). In a form that is convenient for absorption, we write

$$H_a = E_a + \sum_k \hbar\omega_k (a_k^\dagger a_k + \tfrac{1}{2}) , \quad (5a)$$

$$H_b = H_a + \hbar\omega_{ba} + \sum_k (v_k a_k + v_k^* a_k^\dagger)$$

$$+ \tfrac{1}{2} \sum_{kk'} v_{kk'} (a_k + a_k^\dagger)(a_{k'} + a_{k'}^\dagger) , \quad (5b)$$

where $a_k^\dagger$ and a_k are creation and annihilation operators for phonons of mode k having frequency ω_k. v_k and $v_{kk'}$ are linear- and quadratic-coupling coefficients, respectively, and $\hbar\omega_{ba}$ is a static energy difference associated with the $a \to b$ transition, which includes the purely electronic energy difference. To treat emission, a linear transformation of the phonon operators

$$A_k = \sum_{k'} (\phi_{kk'} a_{k'} + \psi_{kk'} a_{k'}^\dagger) + \tau_k \quad (6)$$

can be used to cast the excited- and new initial-state Hamiltonian H_b in the form (5a), and the new final-state Hamiltonian H_a in the form (5b):

$$H_a = H_b - \left(\hbar\Omega_{ba} + \sum_k (V_k A_k + V_k^* A_k^\dagger) \right.$$

$$\left. + \tfrac{1}{2} \sum_{kk'} V_{kk'} (A_k + A_k^\dagger)(A_{k'} + A_{k'}^\dagger) \right) , \quad (7a)$$

$$H_b = E_b + \sum_k \hbar\Omega_k (A_k^\dagger A_k + \tfrac{1}{2}) . \quad (7b)$$

We would like to emphasize that in writing the initial-state Hamiltonian in the simplest harmonic oscillator form, we include some quadratic-coupling effects in the phonon frequencies ω_k and Ω_k and in the linear-coupling coefficients v_k and V_k. This is shown explicitly in the discussion that follows.

A case which goes beyond strictly linear coupling, but one for which the transformation in Eq. (6) can be carried out exactly, occurs when no off-diagonal (mode-mixing) quadratic coupling is retained. This case is simply related to familiar configurational-coordinate models which include quadratic coupling; Appendix A shows how to translate the notation used here into familiar configurational coordinate terms.

With $v_{kk'} = V_{kk'} = 0$ for $k \neq k'$ in Eqs. (5b) and (7a), the ratios γ_k of the phonon frequencies in the excited state to those in the ground state are found to be

$$\gamma_k = \Omega_k / \omega_k = [1 + 2(v_{kk}/\hbar\omega_k)]^{1/2} . \quad (8)$$

Assuming for the sake of simplicity that they are real, the linear-coupling coefficients in the two states are related by

$$V_k = v_k / \gamma_k^{5/2} \quad (9)$$

and the quadratic-coupling coefficients by

$$V_{kk} = v_{kk} / \gamma_k . \quad (10)$$

In this case, the transformation from ground-state phonon operators a_k, $a_k^\dagger$ to excited-state operators A_k, $A_k^\dagger$ is diagonal, with

$$A_k = \phi_k a_k + \psi_k a_k^\dagger + \tau_k , \quad (11)$$

$$\phi_k = (\gamma_k + 1)/2\gamma_k^{1/2} , \quad (12a)$$

$$\psi_k = (\gamma_k - 1)/2\gamma_k^{1/2} , \quad (12b)$$

$$\tau_k = \frac{v_k/\hbar\omega_k}{\gamma_k^{3/2}} . \quad (12c)$$

The three constant energy differences $\hbar\omega_{ba}$, $\hbar\Omega_{ba}$, and $E_b - E_a$ of interest in Eqs. (5a) and (5b) and (7a) and (7b) differ by sums involving the squares of the linear-coupling coefficients, i. e.,

$$\hbar\Omega_{ba} = \hbar\omega_{ba} - \sum_k \gamma_k^{-4} (\gamma_k^2 + 1)(v_k^2/\hbar\omega_k) , \quad (13a)$$

$$E_b - E_a = \hbar\omega_{ba} - \sum_k \gamma_k^{-2} (v_k^2/\hbar\omega_k) . \quad (13b)$$

If there is no quadratic coupling at all, that is, if $v_{kk} = V_{kk} = 0$, then the phonon frequencies in the ground and excited states are the same, $\gamma_k = \Omega_k/\omega_k = 1$, and the phonon operators in the two states are simply displaced from each other, e. g., $A_k = a_k + v_k/\hbar\omega_k$.

B. Approximations to the Spectral Functions

Because of the formal symmetry between the equations for absorption and emission, the methods and approximations used to treat either case apply with only minor modifications to the other. Therefore, in the following, we shall concentrate our attention on absorption, noting from time to time the substitutions to be made for emission.

The absorption function $G(ab; t)$, defined in Eq. (4), is calculated by inserting in that equation the expressions for H_a and H_b given by Eqs. (5a) and (5b). The result is an exponential of an infinite sum of cumulants,[3] whose sum rigorously terminates with the second cumulant if only linear coupling is allowed. When quadratic coupling is included, the higher-order cumulants do not vanish, but contribute corrections involving products of three or more v's, of which at least one must be a quadratic-coupling coefficient $v_{kk'}$. As previously noted, two of the most readily observed physical effects of quadratic coupling are to make the no-phonon linewidth and peak position temperature dependent and to break the mirror symmetry between absorption and emission which occurs in the strict linear-coupling limit. The first of these effects is included by quadratic-coupling terms in the second cumulant, and the second is already implicit in the transformation given by Eq. (6), as may be seen clearly in Eqs. (8)–(10). The higher cumulants are not needed to produce these two important physical effects and, furthermore, since these cumulants begin at first order in the quadratic-coupling coefficients, they are the same for absorption and emission to this order. It would seem, therefore, that the higher-order cumulants can be neglected without serious qualitative consequences, at least for the case of weak quadratic coupling.

With this approximation, $G(ab; t)$ is found to be

$$G(ab; t) = e^{-S} e^{-i\omega_0 t} e^{g_1(t) + g_2(t)} , \qquad (14)$$

where S is the total Huang-Rhys factor for the transition, ω_0 is the no-phonon frequency, and $g_1(t)$ and $g_2(t)$ arise from the linear and quadratic coupling, respectively. In terms of the coupling coefficients, the Bose-Einstein functions

$$n(\omega_k) = (e^{\beta\hbar\omega_k} - 1)^{-1} ,$$

and individual-mode Huang-Rhys factors

$$S_k \equiv |v_k|^2/(\hbar\omega_k)^2 , \qquad (15)$$

the quantities S, ω_0, and $g_1(t)$ are given by

$$S = \sum_k S_k[2n(\omega_k) + 1] , \qquad (16)$$

$$\hbar\omega_0 = \hbar\omega_{ba} - \sum_k \hbar\omega_k S_k + \tfrac{1}{2}\sum_k v_{kk}[2n(\omega_k) + 1] + O(v_{kk'}^2) , \qquad (17)$$

$$g_1(t) = \sum_k S_k\{[n(\omega_k) + 1] e^{-i\omega_k t} + n(\omega_k) e^{i\omega_k t}\} . \qquad (18)$$

We have not given the expression for $g_2(t)$ because it is quite complicated, and we intend to neglect its contributions except in the region $\omega \simeq \omega_0$, where its primary role is to give a temperature-dependent width to the zero-phonon line. The approach used is to simplify the analysis by keeping only the lowest-order terms which yield the qualitative effects of major importance. For this reason we will also

neglect the terms of order $v_{kk'}^2$ in $\hbar\omega_0$ because they are not necessary to give a temperature dependence to the peak position of the zero-phonon line. It should be understood, however, that even though $g_1(t)$ does not contain quadratic-coupling coefficients explicitly, the mirror symmetry between absorption and emission characteristics of pure linear coupling can be broken by quadratic-coupling effects in the transformation described by Eq. (6).

In the no-phonon region where $\omega \simeq \omega_0$, the $|t| \to \infty$ behavior of $g_2(t)$ is most important. It can be shown that in this limit, $g_2(t)$ has the asymptotic form[3,11,13]

$$g_2(t) \sim - \Gamma_0|t| , \qquad (19)$$

where

$$\hbar\Gamma_0 = \pi \sum_{kk'} v_{kk'}^2\, n(\omega_k)\, [n(\omega_k) + 1]\, \delta(\hbar\omega_k - \hbar\omega_{k'}) . \qquad (20)$$

Employing Eq. (19) and keeping only that part of $e^{g_1(t)}$ which does not depend on t, we find that the no-phonon line is a Lorentzian described by

$$G_0(ab; \omega) \simeq e^{-S} [\textstyle\prod_k I_0(c_k)]\{2\Gamma_0/[(\omega - \omega_0)^2 + \Gamma_0^2]\} . \qquad (21)$$

Here,

$$c_k = S_k \operatorname{csch} \tfrac{1}{2}\beta\hbar\omega_k \qquad (22)$$

and $I_0(c_k)$ is a zeroth-order modified Bessel function.

The total broad-band spectrum $G_B(ab; \omega)$, defined here as the entire spectrum minus the zero-phonon contribution, is

$$G_B(ab; \omega) \equiv G(ab; \omega) - G_0(ab; \omega)$$

$$\simeq e^{-S} \int_{-\infty}^{\infty} dt\, e^{i(\omega-\omega_0)t} [e^{g_1(t)} - \textstyle\prod_k I_0(c_k)] . \qquad (23)$$

We have not included the shape of the no-phonon line in this expression because we are most interested in the behavior of $G_B(ab; \omega)$ for frequencies outside the no-phonon region.

Formal series expansions for the broad-band spectral function $G_B(ab; \omega)$ can be obtained for arbitrary temperatures, but these simplify greatly in the limit $T \to 0$ where any vibronic structure present is sharpest. We will therefore seek a detailed picture of $G_B(ab; \omega)$ only for $T \to 0$. In this limit, $n(\omega_k) = 0$, so electronic transitions can be accompanied only by phonon emission. The total Huang-Rhys factor for the impurity reduces to

$$S = \sum_k S_k , \qquad (24)$$

and Eq. (18) becomes simply

$$g_1(t) = \sum_k S_k e^{-i\omega_k t} . \qquad (25)$$

Since now $c_k = 0$ and $I_0(c_k) = 1$, the total broad-band spectrum described by Eq. (23) can be expressed

as a sum of n-phonon spectra by expanding $e^{g_1(t)} - 1$ in powers of $g_1(t)$; thus

$$G_B(ab;\omega) = \sum_{n=1}^{\infty} G_n(ab;\omega) , \qquad (26)$$

with

$$G_n(ab;\omega) = e^{-S} \int_{-\infty}^{\infty} dt\, e^{i(\omega-\omega_0)t} [g_1(t)]^n/n! . \qquad (27)$$

Substitution of Eq. (25) into Eq. (27) with $n=1$ yields the one-phonon spectrum for absorption at $T=0$, namely,

$$G_1(ab;\omega) = 2\pi e^{-S} \sum_k S_k \delta[(\omega-\omega_0) - \omega_k]. \qquad (28)$$

The n-phonon spectrum may be written as an n-fold convolution of the one-phonon spectrum or explicitly in terms of the S_k's and ω_k's,

$$G_n(ab;\omega) = \frac{2\pi e^{-S}}{n!} \int_{-\infty}^{\infty} d\omega_1 \cdots d\omega_n \frac{e^S G_1(ab;\omega_1)}{2\pi} \cdots \frac{e^S G_1(ab;\omega_n)}{2\pi} \delta\left((\omega-\omega_0) - \sum_{m=1}^{n}(\omega_m-\omega_0)\right)$$

$$= 2\pi e^{-S} \sum_{\{n_k \geq 0\}} \delta_{n,\Sigma_k n_k} \cdot \left(\prod_k \frac{S_k^{n_k}}{n_k!}\right) \delta\left((\omega-\omega_0) - \sum_k n_k \omega_k\right) . \qquad (29)$$

An alternative procedure[17] is to express G_n as a convolution of G_1 and G_{n-1} so that

$$G_n(ab;\omega) = (e^S/2\pi n) \int_{-\infty}^{\infty} d\omega_1 G_1(ab;\omega_1)$$

$$\times G_{n-1}(ab;\omega-\omega_1+\omega_0) . \qquad (30)$$

This form is probably more convenient for general applications, although we have used Eq. (29) for the calculations in this paper.

As n increases, whatever structure occurs in the one-phonon spectrum tends to be washed out by the convolution process, making $G_n(ab;\omega)$ smoother for larger n. Moment analysis may therefore be useful for calculating the higher n-phonon spectra. This problem will be considered in detail in Sec. II C, but it seems appropriate here to note a familiar result of such analysis. At $T=0$, the ratio of the integrated intensity of the n-phonon spectrum to the integrated intensity under the total broad-band curve is

$$\frac{\int_{-\infty}^{\infty} d\omega\, G_n(ab;\omega)}{\int_{-\infty}^{\infty} d\omega\, G_B(ab;\omega)} = \frac{S^n}{n!} \frac{e^{-S}}{(1-e^{-S})} . \qquad (31)$$

Equation (31) is valid for all n, including $n=0$, thereby providing a standard measure of the total Huang-Rhys factor at $T=0$.

The equations written so far for absorption can be applied directly to emission, with two modifications. First, as indicated by Eqs. (5a) and (5b) and (7a) and (7b), the absorption frequencies and coupling coefficients ω_k, ω_{ba}, v_k, and $v_{kk'}$ should be replaced by their counterparts for emission Ω_k, Ω_{ba}, V_k, and $V_{kk'}$. The individual-mode Huang-Rhys factors $\mathcal{S}_k$ for emission are

$$\mathcal{S}_k = |V_k|^2/(\hbar\Omega_k)^2 , \qquad (32)$$

and for the case of no off-diagonal quadratic coupling, we find from Eqs. (8), (9), (15), and (32) that

$$\mathcal{S}_k = S_k/\gamma_k^7 . \qquad (33)$$

For weak quadratic coupling,

$$\gamma_k = \Omega_k/\omega_k = [1 + 2(v_{kk}/\hbar\omega_k)]^{1/2}$$

is close to unity, and the phonon frequency shifts between emission and absorption are small. However, weak quadratic coupling produces much larger differences in the individual-mode Huang-Rhys factors and correspondingly in their sum; this is a major factor in breaking the mirror symmetry between absorption and emission. Second, the sign of the photon frequency referred to the no-phonon line should be changed in going from absorption to emission. This can be accomplished directly by letting $\omega-\omega_0 \to -(\omega-\omega_0)$ in expressions for the spectral functions, or indirectly, by replacing ω_k by $-\Omega_k$ everywhere it occurs except as an argument of Bose-Einstein functions.

C. Moment Analysis

The moment analysis approach used to approximate the higher n-phonon absorption spectra at $T=0$ and the total broad-band spectrum as a function of temperature is described here. In order to obtain the desired range of application, we have included the first five moments or cumulants in our analysis.[18,19] Some of the equations involved are rather cumbersome to write down, though easy to use, and since we feel they may be of interest to other workers, we have included them in Appendix B.

For a function $f(\omega)$ defined by [cf. Eq. (4)]

$$f(\omega) = \int_{-\infty}^{\infty} dt\, e^{i\omega t} f(t) , \qquad (34)$$

the area under $f(\omega)$ and the mth moment about the origin are given by

$$F = \int_{-\infty}^{\infty} d\omega\, f(\omega) = 2\pi f(t=0) , \qquad (35)$$

$$\langle \omega^m \rangle = F^{-1} \int_{-\infty}^{\infty} d\omega\, \omega^m f(\omega) = \left[[f(t)]^{-1} \left(i\frac{d}{dt} \right)^m f(t) \right]_{t=0} .$$
(36)

Moments about the mean are defined by $\langle (\Delta\omega)^m \rangle = \langle (\omega - \langle \omega \rangle)^m \rangle$. In particular, the mean frequency and the mean square width, which are often all that are used in simple semiclassical fits to experimental broad-band data, are found from

$$\langle \omega \rangle = \left(i\frac{d}{dt} \ln f(t) \right)_{t=0} ,$$
(37)

$$\langle (\Delta\omega)^2 \rangle = \left[[f(t)]^{-1} \left(i\frac{d}{dt} \right)^2 f(t) \right]_{t=0} .$$
(38)

In terms of the dimensionless variable x,

$$x = (\omega - \langle \omega \rangle)/[\langle (\Delta\omega)^2 \rangle]^{1/2} ,$$
(39)

an asymptotic expansion for $f(\omega)$ is[2,18]

$$f(\omega) = F\,[2\pi \langle (\Delta\omega)^2 \rangle]^{-1/2}\, e^{-x^2/2}$$

$$\times \{ 1 + \gamma_1 f_{11}(x) + [\gamma_2 f_{21}(x) + \gamma_1^2 f_{22}(x)]$$

$$+ [\gamma_3 f_{31}(x) + \gamma_1 \gamma_2 f_{32}(x) + \gamma_1^3 f_{33}(x)] + \cdots \} .$$
(40)

γ_1 and γ_2 are the coefficients of skewness and excess, and γ_3 is the coefficient for the fifth cumulant; the γ_i and the functions $f_{ij}(x)$ are given in Appendix B. We will sometimes refer to curves generated from Eq. (40) as skewed Gaussians, since they reduce to Gaussians when $\gamma_1 = \gamma_2 = \gamma_3 = 0$.

The moments and cumulants of each of the individual n-phonon spectra at $T = 0$ are found [cf. Eqs. (27) and (34)] by using $f(t) = e^{-S} [g_1(t)]^n/n!$ in Eqs. (35)–(38). Similarly, the temperature-dependent broad-band moment parameters are determined by substituting Eqs. (18) and (23) into Eqs. (35)–(38), noting that $S(T) = g_1(t = 0; T)$. These results are given in Appendix B.

If the non-Gaussian corrections in Eq. (40) are neglected, the full width at half-maximum of $f(\omega)$ is

$$\Delta\omega = [8(\ln 2) \langle (\Delta\omega)^2 \rangle]^{1/2} ,$$
(41)

which is sometimes a good approximation even for smooth curves skewed considerably away from a Gaussian line shape. The corresponding approximation for the peak position of $f(\omega)$ is $\omega_{\max} = \langle \omega \rangle$, but this is acceptable much less frequently. The familiar semiclassical, one-configurational-coordinate formulas for the broad-band peak position and half-width can be recovered from the general results in Appendix B by making these approxima-

tions, dropping the summations over modes in Eqs. (B19) and (B20) for $\langle \omega \rangle_B$ and $\langle (\Delta\omega)^2 \rangle_B$ and setting $\delta = 0$ in these expressions. Denoting the frequency and Huang-Rhys factor of the single mode in absorption by ω_g and S_g, we then have

$$\omega_{\max} = \omega_g S_g ,$$
(42)

$$\Delta\omega(0) = [8(\ln 2) S_g]^{1/2} \omega_g ,$$
(43)

$$\Delta\omega(T)/\Delta\omega(0) = (\coth\beta\hbar\omega_g)^{1/2} .$$
(44)

We would like to make several points about the moment analysis results given in this section and Appendix B. First, it can be seen by comparing Eqs. (B10)–(B15) and (B18)–(B23) that at $T = 0$ the n-phonon spectral moments and cumulants are simply related (by factors involving only n and S) to those of the *total* broad-band curve. Estimates from experiment of the broad-band moments may therefore be a valuable aid in attempting to reconstruct the one-phonon spectrum from the total observed spectrum. Second, including the fifth cumulant corrections and others of the same order of magnitude [the γ_3, $\gamma_1 \gamma_2$, and γ_1^3 terms in Eq. (40)] produces noticeable improvements for computational purposes. In some cases, for example, $G_n(ab; \omega)$ can be calculated by moment analysis for at least one lower value of n when these terms are included rather than when they are not. Also, by including them we usually obtain better agreement between the $T = 0$ broad-band curve found by summing the $G_n(ab; \omega)$ and that determined directly by moment analysis. Finally, to apply the moment equations to emission, we can simply replace ω and $\Delta\omega$ by $-\omega$ and $-\Delta\omega$ on the left-hand sides of Eqs. (B11)–(B15) and (B19)–(B23) and substitute Ω_k and S_k for ω_k and S_k on the right-hand sides.

D. Temperature Dependence of the Zero-Phonon Line

The peak position and the half-width of the zero-phonon line depend on temperature through the quadratic-coupling terms in Eqs. (17) and (20). Since reliable information about the $v_{kk'}$ will seldom be available in any case, an approximation which will allow us to estimate their magnitudes without unduly complicating the analysis would be useful. The approximation $v_{kk'} = \alpha v_k v_{k'}$[13,20] has been used in the past, and we suggest a slight generalization of it here. Recalling from Eq. (15) that $|v_k|^2 = (\hbar\omega_k)^2 S_k$, we define dimensionless parameters α_1 and α_2 by

$$\frac{\alpha_1}{\hbar\omega_D} = \frac{\sum_k v_{kk}[2n(\omega_k) + 1]}{\sum_k (\hbar\omega_k)^2 S_k [2n(\omega_k) + 1]} ,$$
(45)

$$\left(\frac{\alpha_2}{\hbar\omega_D} \right)^2 = \sum_{kk'} v_{kk'}^2\, n(\omega_k)[n(\omega_k) + 1]\, \delta(\hbar\omega_k - \hbar\omega_{k'}) \Big/ \sum_{kk'} [(\hbar\omega_k)^2 S_k][(\hbar\omega_{k'})^2 S_{k'}]\, n(\omega_k)[n(\omega_k) + 1]\, \delta(\hbar\omega_k - \hbar\omega_{k'}) ,$$
(46)

where ω_D is an arbitrary characteristic phonon frequency introduced for scaling purposes; for the present problem, a reasonable choice for ω_D might be $\omega_D = \sum_k \omega_k S_k / \sum_k S_k$. In terms of α_1 and α_2, the no-phonon peak position and half-width given in Eqs. (17) and (20) now become

$$\hbar\omega_0 = \hbar\omega_{ba} - \sum_k \hbar\omega_k S_k$$

$$+ (\alpha_1/2\hbar\omega_D)\sum_k (\hbar\omega_k)^2 S_k [2n(\omega_k)+1] \quad (47)$$

and

$$\hbar\Gamma_0 = \pi\left(\frac{\alpha_2}{\hbar\omega_D}\right)^2 \sum_{kk'} [(\hbar\omega_k)^2 S_k][(\hbar\omega_{k'})^2 S_{k'}]$$

$$\times n(\omega_k)[n(\omega_k)+1]\,\delta(\hbar\omega_k - \hbar\omega_{k'}) \,. \quad (48)$$

α_1 and α_2 are functions only of the temperature; they approach constant values at high temperature and vary at low temperature in a manner which reflects how differently the $v_{kk'}$ and the products $v_k v_{k'}$ weight the phonon frequency distribution. Neglecting the temperature dependence of α_1 and α_2 is an approximation much like assuming a single Debye temperature $\Theta(T)$ for two different thermodynamic properties of a crystal. With this approximation, the only phonon parameters needed to calculate the total absorption spectrum $G(ab;\omega)$, including the no-phonon line $G_0(ab;\omega)$, are the phonon frequencies ω_k and Huang-Rhys factors S_k.

Thus far not many experimental studies of the temperature dependence of zero-phonon lines have been made and in the illustrative example considered in Sec. IV nothing will be said about the matter because of lack of experimental data. However, in a paper to follow shortly, the results of a detailed experimental and theoretical study of the absorption and emission bands of one of the M centers in MgF_2 will be given. From that work, it will be seen that the temperature dependence of the position and width of the zero-phonon line is given rather well by Eqs. (47) and (48) within the limits of accuracy of the experimental data.

III. COMPUTATIONAL DETAILS

The starting point for the application of the theory presented in the Sec. II is an estimate of $G_1(ab;\omega)$ at $T=0$ as expressed by Eq. (28). $G_1(ab;\omega)$ is essentially a weighted one-phonon density of states which involves the individual mode frequencies ω_k and Huang-Rhys factors S_k in addition to the total Huang-Rhys factor S. Of course, the ω_k and S_k are generally not known with any precision and, in fact, we would like to extract information about these quantities from the experimental data. In principle, we can derive $G_1(ab;\omega)$ from the observed broad-band spectrum at $T=0$ simply by subtracting from $G_B(ab;\omega)$ the sum of the n-phonon spectra for $n \geq 2$. (It should be remembered that G_B does not contain

the no-phonon contribution.) However, since $G_1(ab;\omega)$ is needed in order to generate the G_n contained in G_B, some type of iterative procedure is called for. One can be set up as follows. Given an initial estimate of the effective one-phonon spectrum, G_B is calculated and compared with the experimental curve. If the results are not satisfactory, a new one-phonon spectrum is obtained by calculating the sum of the G_n for $n \geq 2$ and subtracting the resulting curve from the experimental one. This process is then repeated until satisfactory results are achieved. In practice, such a simple procedure encounters some problems, including the occasional prediction of negative Huang-Rhys factors, and, as a consequence, it is difficult to fully automate it for a computer.

A *starting* one-phonon spectrum may be found in several ways. In cases where one has reason to believe that most of the vibronic structure is due to one-phonon processes, an intuitive approach in which the spectrum is roughly estimated from the experimental data may be adequate. A perfect crystal density of states ρ_0, or various symmetry projections of it, when these are available, may be useful in determining a first approximation to $G_1(ab;\omega)$. If neither of these methods is viable, as may be the case when relatively little vibronic structure is superimposed on a smooth broad band, moment analysis may be extremely useful in the following way. The first two moments of the total experimental curve can be estimated from the peak position and the half-width. Since there is a simple relationship between the broad-band moments and the moments of the n-phonon processes for every value of n, a Gaussian-like one-phonon spectrum can be readily obtained. This spectrum will of course not have any pronounced structure, but it will have the virtue of giving the first two moments of the experimental curve rather well. A refinement of the effective one-phonon density of states which does contain structure is then found by subtracting the calculated sum of $G_n(ab;\omega)$ for $n \geq 2$ from the experimental curve as discussed above for the iterative procedure.

The model assumed for numerical calculations might be thought of as being based on a kind of many-configurational-coordinate picture. The roughly 10^{23} phonon modes of the crystal are replaced by a finite but large number of modes, evenly spaced in frequency, with the sum of the strengths S_k normalized to the total Huang-Rhys factor at $T=0$. However, a more general approach can be set up by defining a function $S(\omega)$,

$$S(\omega) = \sum_k S_k \delta(\omega - \omega_k) \,, \quad (49)$$

which, since S_k is dimensionless, has the dimensions of the usual density of states. In transforming the formulas given in terms of S_k, ω_k, and

sums over k to expressions involving $S(\omega)$, ω, and integrals over ω, the factor $\prod_k I_0(c_k)$ causes the only problem, and then only for $T \neq 0$. If moment analysis is to have any utility for determining broad-band characteristics as functions of temperature, however, this factor is relatively unimportant. In any event, an alternative way of arriving at the model to be used is to replace the continuous effective density of states $S(\omega)$ by a series of evenly spaced δ functions:

$$S(\omega) = \sum_k S_k \, \delta(\omega - k\Delta) \, . \qquad (50)$$

The set of strengths S_k and the frequency interval Δ are the only nontrivial inputs for the calculations in a single iteration.

At $T = 0$, the lower n-phonon spectra are generated for each value of n both by convoluting the one-phonon spectrum according to Eq. (29) or (30) and by moment analysis from Eqs. (39) and (40) and (B1)–(B15). The convolution process is stopped once an rms difference comparison of the two methods shows that moment analysis is adequate for larger values of n. The total broad-band spectrum is then given as the sum of the $G_n(ab; \omega)$. All results are plotted by connecting consecutive points (δ-function strengths) with straight lines; as drawn, the curves rigorously satisfy rule (31) for the ratios of the integrated intensities at $T = 0$.

A few remarks on the computer time required by our program may be of interest. The amount of machine time depends primarily on the number of δ-function spikes used to represent the one-phonon spectrum and on the value of n at which it becomes possible to determine the n-phonon spectrum by moment analysis. The total number of terms in the sum on the right-hand side of Eq. (29) or (30) is a rapidly increasing function both of the number of spikes m, and the number of phonons. In terms of computer time with our codes, calculating the n-phonon spectra through $n = 3$ for $m = 100$ by convoluting the one-phonon spectrum according to Eq. (29) takes a few seconds on the IBM 360-91. The computer time also depends on the magnitude of the total Huang-Rhys factor, since the vibronic structure tends to disappear as S increases. Thus, although the structure in the lower n-phonon spectra may be quite pronounced, it contributes less to the total spectrum as S increases. This means that for larger S the decision about the value of n at which to use moment analysis for $G_n(ab; \omega)$ is not very crucial.

As already noted, emission can be treated in the same way as absorption, but with a different one-phonon spectrum $\{\Omega_k, \mathcal{S}_k\}$ and a change in the sign of the photon frequency referred to the no-phonon line. An emission spectrum could be obtained in exactly the manner described above for absorption, but the more interesting problem is to attempt a description of both emission and absorption within a unified framework. As a first step toward this objective, we will neglect off-diagonal quadratic coupling and use Eqs. (9)–(13b) and (33), which are exact in this approximation, to relate the emission and absorption spectra. Although this simplifies matters considerably, there remains the problem of determining the diagonal coupling coefficients v_{kk}. We would like to express these coefficients in terms of the more accessible parameters we have been working with through most of the discussion, namely, ω_k and S_k (or Ω_k and $\mathcal{S}_k$). Two simple approximations are suggested in the literature.[3,13,20]

In the first of these, it is assumed that

$$v_{kk} = \epsilon \hbar \omega_k \, , \qquad (51)$$

where ϵ is a proportionality constant which is the same for all k. This applies directly for band modes in the long-wavelength limit and may be adequate for our purposes for all modes. Substituting (51) into Eqs. (8) and (33), we find that the phonon frequencies and Huang-Rhys factors for emission are related to those for absorption in this approximation by

$$\Omega_k = \gamma_0 \omega_k \, , \qquad (52)$$

$$\mathcal{S}_k = S_k / \gamma_0^7 \, , \qquad (53)$$

where

$$\gamma_0 = (1 + 2\epsilon)^{1/2} \, . \qquad (54)$$

Since ω_k and S_k are simply multiplied by constants in Eqs. (52) and (53), this is a particularly convenient model to use for calculations.

The second possibility, already touched on in the discussion of the zero-phonon line, is to assume that the quadratic-coupling coefficients are proportional to the squares of the linear-coupling coefficients,

$$v_{kk} = (\alpha / \hbar \omega_D) |v_k|^2 = (\alpha / \hbar \omega_D)(\hbar \omega_k)^2 S_k \, . \qquad (55)$$

Here, as in Eqs. (45) and (46), $\hbar \omega_D$ has been introduced to make α dimensionless. Equations (8) and (33) for the phonon parameters in emission are unchanged, but γ_k is now given by

$$\gamma_k = [1 + 2\alpha(\omega_k / \omega_D) S_k]^{1/2} \, . \qquad (56)$$

In the model used for numerical calculations, this is a slightly less convenient approximation than the preceding one, and we have not found it necessary to employ it in this paper. It does have the advantage, however, of predicting relatively larger quadratic coupling for those modes which have the strongest linear-coupling coefficients, which seems intuitively reasonable.

IV. RESULTS OF AN EXAMPLE

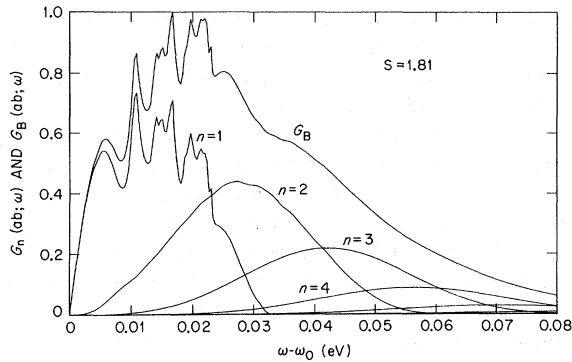The defect we will use to illustrate our approach is the N_1 color center in NaCl, which has been

FIG. 1. The calculated total broad-band spectrum and its n-phonon components at $T = 0$. The curves in this and all succeeding figures were drawn by a Calcomp plotter.

studied experimentally by Hughes[21] and Pierce.[22] From stress splitting measurements on the zero-phonon line of the observed electronic transition, they conclude that this defect has monoclinic I symmetry, and may be an aggregate of either two or four F centers. The low-temperature absorption spectrum for this transition exhibits a very large amount of vibronic structure and thus provides a good test of the methods described above for the calculation of $G_B(ab; \omega)$ at $T = 0$. However, due to insufficient experimental information available to us for this center, we cannot illustrate the calculations of the temperature dependence of the no-phonon parameters. As previously mentioned, a combined experimental and theoretical study of the optical spectra of one of the M centers in MgF_2 will appear separately, and this will include an analysis of these parameters.

Our final result for the effective one-phonon spectrum for absorption by the N_1 center is shown in Fig. 1. It is constructed from 99 spikes, with an interspike spacing of $\Delta = 0.05 \times 10^{13}$ rad/sec ($= 0.329$ meV) and a total Huang-Rhys factor of $S = 1.81$. The figure also shows the calculated total broad-band absorption spectrum $G_B(ab; \omega)$, as well as all other n-phonon contributions of importance. As Hughes conjectures, most of the observed structure arises from the one-phonon spectrum. However, our calculation shows that the last broad peak is mainly due to one- and two-phonon contributions, and not to four-phonon processes involving the first peak in the one-phonon curve as Hughes suggests. Three-phonon processes give rise to the hump between 0.03 and 0.04 eV, and the background on which the structure is superimposed comes primarily from the one-, two-, and three-phonon spectra. Moment analysis was used to determine $G_n(ab; \omega)$ for $n \geq 4$, and, in fact, might well have been used for $n = 3$ also. The low-frequency tail of the four-phonon curve does extend into the

region where structure occurs, and the n-phonon processes where $n = 4$ or higher determine the shape of the total spectrum at larger values of $\omega - \omega_0$, so that these contributions cannot be neglected.

Figure 2 compares the calculated and experimental results for $G_B(ab; \omega)$. Both curves were drawn by connecting δ-function spikes, separated by 0.329 meV, with straight lines. Experimental values for $G_B(ab; \omega)$ were taken from Hughes's results[23] for $\omega G(ab; \omega)$, using his Fig. 4 for $\omega - \omega_0 = 0$ out to just beyond the last peak, and his Fig. 1 for the remainder. In putting together the information from the two figures, we encountered some uncertainties in matching, and the high-frequency part of the experimental spectrum obtained after dividing by ω is not as well determined as it is in the region where structure appears. Since Hughes gives no precise value for the no-phonon peak height, we simply made a linear extrapolation of $\omega G_B(ab; \omega)$ to 0 at $\omega = \omega_0$ in order to subtract out the no-phonon line, so the experimental curve for $G_B(ab; \omega)$ is also somewhat uncertain for small $\omega - \omega_0$. The calculated and experimental curves cannot be distinguished from one another over the whole range in which vibronic structure occurs, and only minor differences are apparent in the higher-frequency region where our extraction of the experimental results from Hughes's paper is not completely reliable.

Given the one-phonon spectrum in Fig. 1, it took less than two seconds on an IBM 360-91 to generate all of the other curves in that figure and in Fig. 2. With this kind of time factor for each iteration, it was possible to do a large number of them to obtain the final fit to experimental results. The starting one-phonon spectrum included 24 peaks proportional to $\rho_0(\omega)/\omega^2$, with $\rho_0(\omega)$ taken from Hughes's plot of the results of Karo and Hardy.[24] Several iterations were done with 24 peaks in the one-phonon spectrum, the number of peaks was doubled, several more iterations were performed, and the number of peaks was doubled again. The last 40 or so iter-
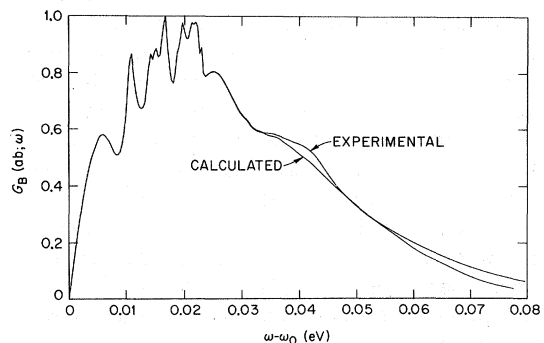

FIG. 2. Calculated and experimental results for $G_B(ab; \omega)$ at $T = 0$.
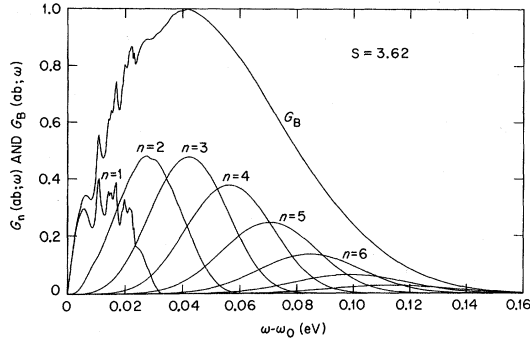
FIG. 3. The spectrum and its components at $T = 0$ when the total Huang-Rhys factor is doubled.

ations were typically done in groups of 4 or 5 at constant values of S, and the only external intervention required was to change S in successively smaller intervals. Although the details of the iterative procedure may vary to some extent with the center and with the experimental resolution, which for this example is excellent, it should be clear that the starting one-phonon spectrum is not crucial to the final results, and that a major feature of the fitting procedure is the determination of the total Huang-Rhys factor S. To further emphasize this last point, Fig. 3 shows the total and the n-phonon spectra produced by the same one-phonon spectrum as in Fig. 1 but with twice the total Huang-Rhys factor. Vibronic structure is still present in $G_B(ab; \omega)$, but it is much less pronounced and is superimposed on the low-frequency side of a more Gaussian-like broad band. Figure 4 compares the total curve in Fig. 3 with the corresponding moment-analysis result, and it can be seen that the skewed Gaussian curve is a reasonably good approximation to the over-all line shape. For S of the order of 4 or higher, moment analysis should generally give acceptable values for the temperature dependence of the broad-band half-width.

We have not seen any experimental studies of emission by the NaCl N_1 center, but we can demonstrate how asymmetry between absorption and emission might arise. For this purpose, we neglect off-diagonal coupling and assume $v_{kk} \propto \omega_k$, so that Eqs. (52)–(54) describe the relationship between the one-phonon spectra for emission and absorption. Figure 5 shows the results obtained when the phonon frequencies for emission and absorption are the same or differ by 10% in either direction. With no quadratic coupling, the absorption and emission functions $G_B(ab; \omega)$ and $G_B(ba; \omega)$ are indeed mirror images about the no-phonon line, as seen in Fig. 5(b). If the phonon frequencies in emission are lower by 10%, $\gamma_0 = \Omega_k / \omega_k = 0.90$, the individual-mode Huang-Rhys factors s_k and the total s are larger by more than 100%, $s_k/S_k = s/S = 1/\gamma_0^7$

$= 2.09$. As shown in Fig. 5(a), the emission spectrum is then broader than the absorption spectrum, and vibronic structure is much less pronounced. The reverse situation is presented in Fig. 5(c), which reflects positive quadratic coupling sufficient to increase the phonon frequencies in emission by 10%, $\gamma_0 = \Omega_k / \omega_k = 1.10$, and to reduce the Haung-Rhys factors by about 50%, $s_k/S_k = s/S = 1/\gamma_0^7 = 0.513$. For this case, the emission spectrum is narrower than the absorption spectrum, and the vibronic structure is somewhat more pronounced. Figure 5 vividly demonstrates that relatively small amounts of quadratic coupling can produce substantial asymmetry between absorption and emission.

It is instructive to compare the one-phonon spectrum for absorption with several perfect lattice functions. Figures 6(a)–6(c) show the comparison between $G_1(ab; \omega)$ from Fig. 1 and the perfect lattice distributions $\rho_0(\omega)$, $\rho_0(\omega)/\omega$, and $\rho_0(\omega)/\omega^2$ calculated from a shell model fitted to neutron scattering data.[25] With the exception of the first broad peak in $G_1(ab; \omega)$, the structure in the one-phonon spectrum corresponds rather well to that seen in the perfect lattice density-of-states functions; as both Hughes and Pierce remark, this first peak is probably due to pseudolocalized (resonant) modes. Not surprisingly, $G_1(ab; \omega)$ is not well approximated in detail by any of the three perfect lattice curves, but the over-all fit is clearly better for $\rho_0(\omega)/\omega$ and $\rho_0(\omega)/\omega^2$ than for $\rho_0(\omega)$ itself. The usual comparison made is between $\rho_0(\omega)$ and $\omega^2 G(ab; \omega)$,[13,20,26] which is recast in Fig. 6(c) as a comparison between $G_1(ab; \omega)$ and $\rho_0(\omega)/\omega^2$. Only $\rho_0(\omega)/\omega^2$ actually has a peak corresponding to the second peak in the one-phonon spectrum, but from quite general considerations $\rho_0(\omega)/\omega^2$ approaches a constant at $\omega = 0$ while $G_1(ab; \omega)$ should go linearly to zero. Furthermore, above $\nu \simeq 3 \times 10^{12}$ Hz, $\rho_0(\omega)/\omega$ seems to be slightly closer to $G_1(ab; \omega)$ than is $\rho_0(\omega)/\omega^2$. Returning to a point discussed briefly in Sec. III, the best choice for a *starting* one-phonon spectrum
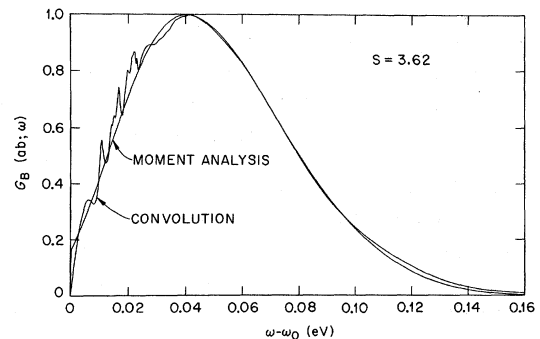

FIG. 4. Comparison of the total curve in Fig. 3. with the corresponding moment analysis result.
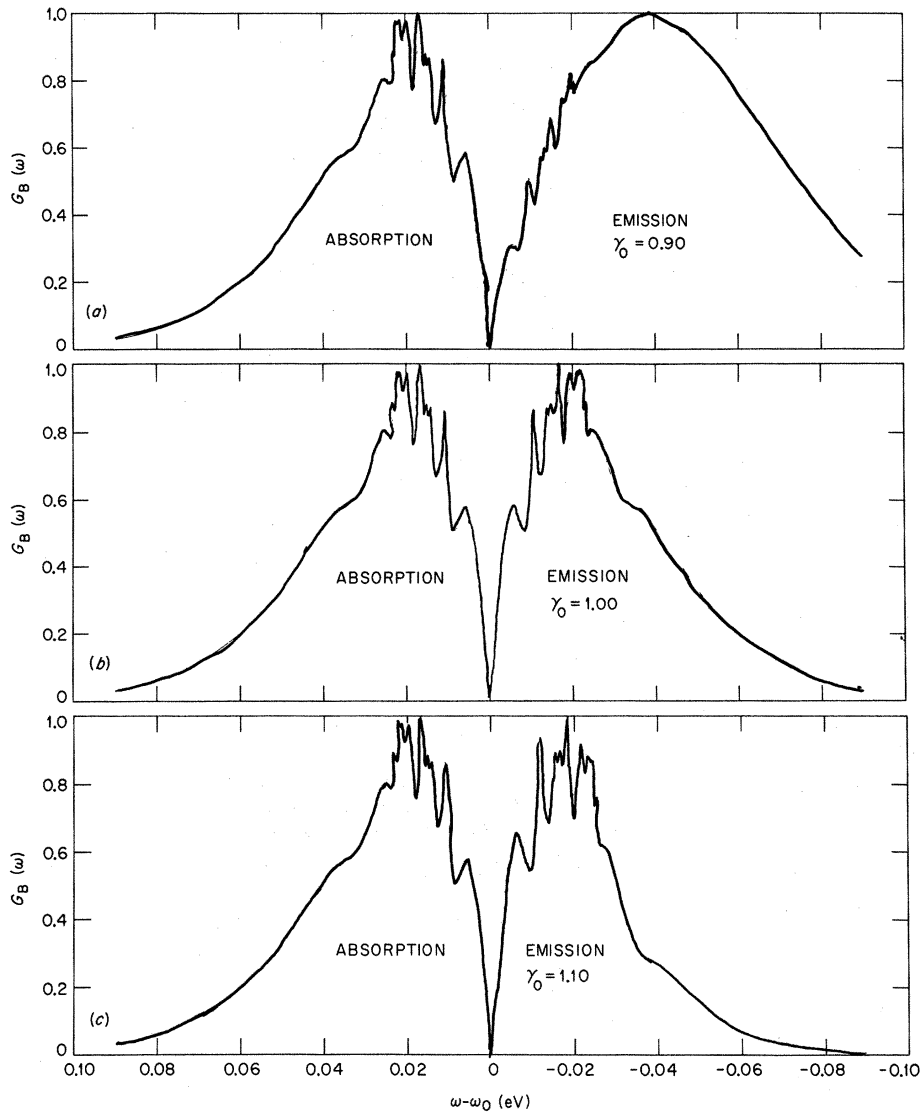
FIG. 5. Emission and absorption spectra for three values of the quadratic coupling parameter $\gamma_0 = \Omega_k/\omega_k$.

would thus appear to be $G_1(ab; \omega) \propto \rho_0(\omega)/\omega^l$, where $1 \le l < 2$.

V. DISCUSSION

Our objective in the work reported in this paper was the development of a computational approach and computer programs to implement it which would enable us to apply the theory of vibronic structure of impurity-related optical spectra to a wide variety of systems. The results of preliminary testing on the N_1 center in NaCl reported herein and on one of the M centers in MgF_2 to be reported in a later paper have been quite encouraging. Further testing on other systems is in progress. Significant features of the work are (i) an iterative procedure to extract an effective one-phonon density of states from experimental data; (ii) the combination of moment analysis and convolution integrals to increase the efficiency of the foregoing; and (iii) the inclusion of quadratic-coupling effects in an approximate but probably quite useful manner.

The essentially exact fit between the calculated and experimental results for the N_1 center in the region where vibronic structure occurs may raise a few questions. First, one might wonder if any arbitrary "experimental" curve can be fitted with the same accuracy. In a completely trivial sense this is indeed the case, because by assuming that the whole spectrum is due entirely to one-phonon processes an exact fit can always be forced. A total Huang-Rhys factor S and individual mode S_k's could be found, with $S \ll 1$, in order that $G_B(\omega) = G_1(\omega)$ [see Eq. (31)]. However, such trivial results can easily be ruled out for a variety of reasons. For example, the value of S found in this way would give quite unreasonable results for the
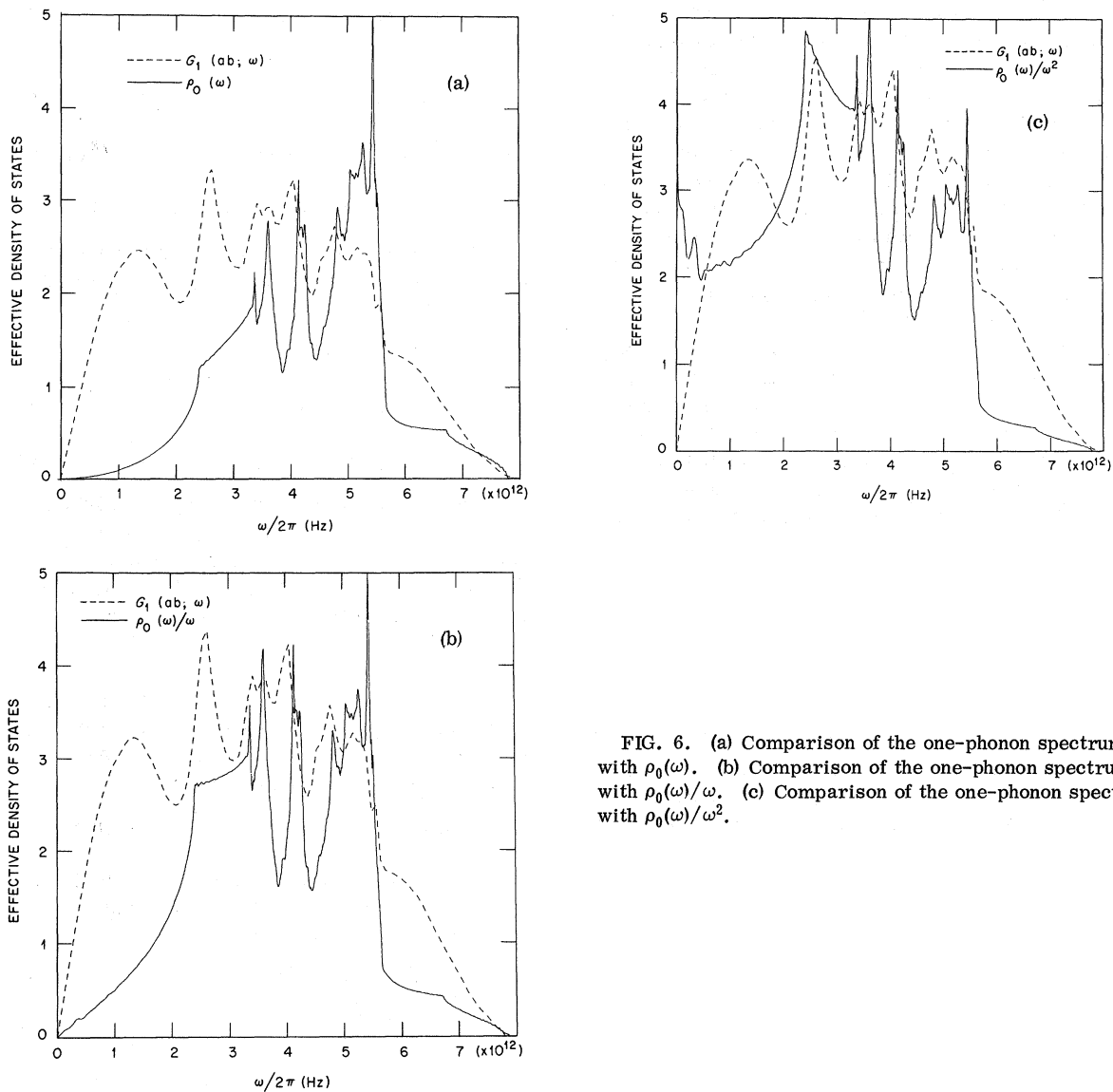
FIG. 6. (a) Comparison of the one-phonon spectrum with $\rho_0(\omega)$. (b) Comparison of the one-phonon spectrum with $\rho_0(\omega)/\omega$. (c) Comparison of the one-phonon spectrum with $\rho_0(\omega)/\omega^2$.

strength of the no-phonon line, and the temperature dependence of the broad-band half-width would be wrong. Also, the frequency range spanned by the perfect lattice density of states would bear no relation to that of the derived one-phonon spectrum. Our procedure does not impose the requirement that the ranges of the one-phonon spectrum and the perfect crystal density of states coincide, although we do expect fairly close coincidence in a variety of cases. For the NaCl N_1 center, for example, our derived $G_1(ab; \omega)$ covers the same frequency range as $\rho_0(\omega)$, whereas the total spectrum covers a range more than twice as great. The same kind of fit to experiment with a broader one-phonon spectrum cannot be approached without increasing the one-phonon frequency range by 40 to 50% or more and, correspondingly, reducing the Huang-

Rhys factor to 1.3–1.2 or lower, which represents a substantial move toward the kind of trivial fit described at the beginning of the paragraph.

A second question concerns the uniqueness of the one-phonon spectrum obtained by our fitting procedure. The answer must depend to some extent on the shape of the observed spectrum, the experimental resolution, and the amount of vibronic structure present. For the Gaussian-like broad bands with no structure which occur for large values of S, it is clearly impossible to work backwards from the total curve to find a unique one-phonon spectrum. Furthermore, one should rely not only on the observed broad-band spectrum at $T = 0$ for a given center, but also on whatever other information and physical insight can be brought to bear on the problem. For example, as noted above,

there is a correlation between the value of the total Huang-Rhys factor and the width of the one-phonon spectrum that gives the "best fit" for that value, although that "best fit" may be unacceptable, since it is, of course, not possible to obtain satisfactory results with arbitrary S values or frequency ranges. To test the sensitivity of our results to the starting one-phonon spectrum, we have generated essentially the same final results for one center by beginning with quite different trial spectra, subject only to the constraint that the Huang-Rhys factor be within reasonable limits of the value estimated from the zero-phonon intensity. Starting from both a smooth one-phonon curve generated by moment analysis and a highly structured curve obtained intuitively from experimental data, we arrived at final one-phonon spectra which were virtually indistinguishable. In summary then, the answer to the question of uniqueness depends on the quality, quantity, and detail of the information available.

We would like to conclude by mentioning a few applications and extensions of the calculational procedure we have described. One possibility is to study the defect-lattice interaction in greater detail by combining the present treatment with a first-principles calculation of coupling coefficients. It should not be difficult to extend the methods used to determine the broad-band spectrum at $T = 0$ to nonzero temperatures, or to amend the computational model to smooth out the calculated curves by giving a width to the δ-function spikes. Finally, in order to deal with a larger number of impurities and defects, it would be necessary to try to apply the same kinds of techniques to systems where orbital degeneracy is an important factor. The basic theory for such centers already exists,[3] and we plan to try to extend our approach to cover these cases in the near future.

APPENDIX A: ONE-CONFIGURATIONAL-COORDINATE MODEL

We consider here the single-configurational-coordinate model for an interacting defect-lattice system in order to show how it relates to the more general approach. In the notation of Klick, Patterson, and Knox,[27] one-configurational-coordinate Hamiltonians for the ground and excited states may be written as

$$H_a = p^2/2m + \tfrac{1}{2}K_g X^2 , \tag{A1a}$$

$$H_b = E_0 + p^2/2m + \tfrac{1}{2}K_e(X - X_0)^2 . \tag{A1b}$$

The ground- and excited-state phonon frequencies are $\omega_g = (K_g/m)^{1/2}$ and $\omega_e = (K_e/m)^{1/2}$. Introducing phonon creation and destruction operators in the usual way, i.e.,

$$X = (\hbar/2m\omega_g)^{1/2}(a + a^\dagger) , \tag{A2a}$$

$$p = -i(\tfrac{1}{2}m\hbar\omega_g)(a - a^\dagger) , \tag{A2b}$$

we obtain

$$H_a = \hbar\omega_g(a^\dagger a + \tfrac{1}{2}) , \tag{A3}$$

$$H_b = H_a + E_0 + \tfrac{1}{2}K_e X_0^2 - K_e X_0 (\hbar\omega_g/2K_g)^{1/2}(a + a^\dagger) $$
$$+ \tfrac{1}{2}[(K_e - K_g)/2K_g]\hbar\omega_g(a + a^\dagger)^2 . \tag{A4}$$

We now define an energy $\hbar\omega_{ba}$ and linear- and quadratic-coupling coefficients v_1 and v_2 (dimensionally also energies) by

$$\hbar\omega_{ba} = E_0 + \tfrac{1}{2}K_e X_0^2 , \tag{A5}$$

$$v_1 = -(\hbar\omega_g/2K_g)^{1/2}K_e X_0 , \tag{A6}$$

$$v_2 = [(K_e - K_g)/2K_g]\hbar\omega_g . \tag{A7}$$

The quadratic-coupling coefficient v_2 vanishes if $K_e = K_g$, or equivalently, if the ground- and excited-state frequencies ω_g and ω_e are the same. The linear coupling is zero if $X_0 = 0$. In terms of $\hbar\omega_{ba}$, v_1, and v_2, Eq. (A4) takes the simple form

$$H_b = H_a + \hbar\omega_{ba} + v_1(a + a^\dagger) + \tfrac{1}{2}v_2(a + a^\dagger)^2 . \tag{A8}$$

It may now be observed that, except for a shift in the energy origin, the more general Hamiltonian definitions (5a) and (5b) reduce to Eqs. (A3) and (A8) for the case of a single mode.

APPENDIX B: MOMENT-ANALYSIS EQUATIONS

The coefficients γ_i in the moment-analysis expansion (40) for $f(\omega)$ are defined in terms of the central moments of $f(\omega)$ by

$$\gamma_1 = \langle(\Delta\omega)^3\rangle/[\langle(\Delta\omega)^2\rangle]^{3/2} , \tag{B1}$$

$$\gamma_2 = \{\langle(\Delta\omega)^4\rangle - 3[\langle(\Delta\omega)^2\rangle]^2\}/[\langle(\Delta\omega)^2\rangle]^2 , \tag{B2}$$

$$\gamma_3 = [\langle(\Delta\omega)^5\rangle - 10\langle(\Delta\omega)^3\rangle\langle(\Delta\omega)^2\rangle]/[\langle(\Delta\omega)^2\rangle]^{5/2} . \tag{B3}$$

The functions $f_{ij}(x)$ in Eq. (40) are

$$f_{11}(x) = \tfrac{1}{6}x(x^2 - 3) , \tag{B4}$$

$$f_{21}(x) = \tfrac{1}{24}(x^4 - 6x^2 + 3) , \tag{B5}$$

$$f_{22}(x) = \tfrac{1}{72}(x^6 - 15x^4 + 45x^2 - 15) , \tag{B6}$$

$$f_{31}(x) = \tfrac{1}{120}x(x^4 - 10x^2 + 15) , \tag{B7}$$

$$f_{32}(x) = \tfrac{1}{144}x(x^6 - 21x^4 + 105x^2 - 105) , \tag{B8}$$

$$f_{33}(x) = \tfrac{1}{1296}x(x^8 - 36x^6 + 378x^4 - 1260x^2 + 945) . \tag{B9}$$

For convenience, all photon frequencies are referred to the no-phonon frequency ω_0 in what follows. In particular, the broad-band and n-phonon

mean frequencies which appear below are measured from ω_0.

The moments and cumulants of the individual n-phonon spectra at $T = 0$, found by using $f(t) = e^{-S} \times [\,g_1(t)]^n/n!$ in Eqs. (35)–(38), are as follows (a subscript n is implied on all angular brackets, the sums run over modes k, and $N \equiv n/S$):

$$F = 2\pi e^{-S} S^n/n! \ , \tag{B10}$$

$$\langle \omega \rangle = N\sum \omega_k S_k \ , \tag{B11}$$

$$\langle (\Delta\omega)^2 \rangle = N\sum \omega_k^2 S_k - \langle \omega \rangle^2/n \ , \tag{B12}$$

$$\gamma_1 [\,\langle (\Delta\omega)^2 \rangle\,]^{3/2} = N\sum \omega_k^3 S_k - 3\langle (\Delta\omega)^2 \rangle \langle \omega \rangle/n^2 - \langle \omega \rangle^3/n^2 \ , \tag{B13}$$

$$\gamma_2 [\,\langle (\Delta\omega)^2 \rangle\,]^2 = N\sum \omega_k^4 S_k - \{4\langle (\Delta\omega)^3 \rangle \langle \omega \rangle + 3[\,\langle (\Delta\omega)^2 \rangle\,]^2\}/n - 6\langle (\Delta\omega)^2 \rangle \langle \omega \rangle^2/n^2 - \langle \omega \rangle^4/n^3 \ , \tag{B14}$$

$$\gamma_3 [\,\langle (\Delta\omega)^2 \rangle\,]^{5/2} = N\sum \omega_k^5 S_k - 5\{\langle (\Delta\omega)^4 \rangle - 3[\,\langle (\Delta\omega)^2 \rangle\,]^2\}\langle \omega \rangle/n - 10\langle (\Delta\omega)^3 \rangle \langle (\Delta\omega)^2 \rangle/n$$
$$- \{10\langle (\Delta\omega)^3 \rangle \langle \omega \rangle^2 + 15[\,\langle (\Delta\omega)^2 \rangle\,]^2 \langle \omega \rangle\}/n^2 - 10\langle (\Delta\omega)^2 \rangle \langle \omega \rangle^3/n^3 - \langle \omega \rangle^5/n^4 \ . \tag{B15}$$

The temperature-dependent broad-band moment parameters follow from Eqs. (18), (23), and (35)–(38). Defining factors δ and A by

$$F_B = 2\pi(1 - \delta) \ , \tag{B16}$$

$$\langle \omega \rangle = A\sum \omega_k S_k \ , \tag{B17}$$

we obtain the following results (a subscript B on all $\langle\rangle$ is suppressed and the sums again run over k):

$$F_B = 2\pi(1 - \delta) \ , \tag{B18}$$

$$\langle \omega \rangle = A\sum \omega_k S_k \ , \tag{B19}$$

$$\langle (\Delta\omega)^2 \rangle = A\sum \omega_k^2 S_k [2n(\omega_k) + 1] - \delta\langle \omega \rangle^2 \ , \tag{B20}$$

$$\gamma_1 [\,\langle (\Delta\omega)^2 \rangle\,]^{3/2} = A\sum \omega_k^3 S_k - \delta\{3\langle (\Delta\omega)^2 \rangle \langle \omega \rangle - (1 - 2\delta)\langle \omega \rangle^3\} \ , \tag{B21}$$

$$\gamma_2 [\,\langle (\Delta\omega)^2 \rangle\,]^2 = A\sum \omega_k^4 S_k [2n(\omega_k) + 1] - \delta\{4\langle (\Delta\omega)^3 \rangle \langle \omega \rangle + 3[\,\langle (\Delta\omega)^2 \rangle\,]^2 - 6(1 - 2\delta)\langle (\Delta\omega)^2 \rangle \langle \omega \rangle^2 + (1 - 6\delta + 6\delta^2)\langle \omega \rangle^4\} \ , \tag{B22}$$

$$\gamma_3 [\,\langle (\Delta\omega)^2 \rangle\,]^{5/2} = A\sum \omega_k^5 S_k - \delta\{5[\,\langle (\Delta\omega)^4 \rangle - 3(\langle (\Delta\omega)^2 \rangle)^2]\langle \omega \rangle + 10\langle (\Delta\omega)^3 \rangle \langle (\Delta\omega)^2 \rangle - 10(1 - 2\delta)\langle (\Delta\omega)^3 \rangle \langle \omega \rangle^2$$
$$- 15(1 - 2\delta)[\,\langle (\Delta\omega)^2 \rangle\,]^2 \langle \omega \rangle + 10(1 - 6\delta + 6\delta^2)\langle (\Delta\omega)^2 \rangle \langle \omega \rangle^3 - (1 - 14\delta + 36\delta^2 - 24\delta^3)\langle \omega \rangle^5\} \ . \tag{B23}$$

In the last four of these expressions, the first term is the dominant one if the total Huang-Rhys factor $S(T)$ is appreciably greater than unity. If δ is set equal to zero, then Eqs. (B18)–(B23) give the moments and cumulants of the total absorption curve $G(ab; \omega)$, rather than just its broad-band part $G_B(ab; \omega) = G(ab; \omega) - G_0(ab; \omega)$.

[1]By point imperfections we mean to include substitutional and interstitial impurities and lattice defects of the color center type; terms such as impurity, defect, and center will be used interchangeably.

[2]M. Lax, J. Chem. Phys. **20**, 1752 (1952).

[3]D. E. McCumber, J. Math. Phys. **5**, 221 (1964); **5**, 508 (1964); Phys. Rev. **136**, A954 (1964); **135**, A1676 (1964).

[4]K. Huang and A. Rhys, Proc. Roy. Soc. (London) **204A**, 406 (1950).

[5]S. I. Pekar, Zh. Eksperim. i Teor. Fiz. **20**, 510 (1950); **22**, 641 (1952).

[6]F. E. Williams, J. Chem. Phys. **19**, 457 (1951); Phys. Rev. **82**, 281 (1951).

[7]R. C. O'Rourke, Phys. Rev. **91**, 265 (1953).

[8]T. H. Keil, Phys. Rev. **140**, A601 (1965).

[9]J. J. Markham, Rev. Mod. Phys. **31**, 956 (1959).

[10]Yu. E. Perlin, Usp. Fiz. Nauk **80**, 553 (1963) [Sov. Phys. Usp. **6**, 542 (1964)].

[11]M. A. Krivoglaz, Fiz. Tverd. Tela **6**, 1707 (1964) [Sov. Phys. Solid State **6**, 1340 (1964)].

[12]E. D. Trifonov, Fiz. Tverd. Tela **6**, 462 (1964) [Sov. Phys. Solid State **6**, 366 (1964)].

[13]A. A. Maradudin, in *Solid State Physics*, Vol. 18, edited by F. Seitz and D. Turnbull (Academic, New York, 1966), p. 273.

[14]D. B. Fitchen, in *Physics of Color Centers*, edited by W. Beall Fowler (Academic, New York, 1968), p. 293.

[15]Here, singlet denotes an orbitally nondegenerate electronic state, or a member of a multiplet whose states are not mixed by the electron-phonon coupling.

[16]D. L. Dexter, in *Solid State Physics*, Vol. 6, edited

by F. Seitz and D. Turnbull (Academic, New York, 1958), p. 353.

[17]J. T. Ritter, J. Chem. Phys. 53, 3461 (1970).

[18]*Handbook of Mathematical Functions with Formulas, Graphs, and Mathematical Tables*, 3rd ed., Natl. Bur. Std. Appl. Math. Ser. 55, edited by M. Abramowitz and I. A. Stegun (U. S. GPO, Washington, D. C., 1965), pp. 928–935.

[19]*Formulae and Tables for Statistical Work*, edited by C. R. Rao, S. K. Mitra, and A. Matthai (Statistical Publishing Society, Calcutta, India, 1966).

[20]G. F. Imbusch. W. M. Yen, A. L. Schawlow, D. E. McCumber, and M. D. Sturge, Phys. Rev. 133, A1029 (1964).

[21]A. E. Hughes, Proc. Phys. Soc. (London) 87, 535 (1966).

[22]C. B. Pierce, Phys. Rev. 148, 797 (1966).

[23]Although Hughes's curves are densitometer traces, the experimental procedures followed were such that the results should be proportional to the absorption coefficient, or nearly so [A. E. Hughes (private communication)]. In any case, the quantitative significance of the experimental results is not of major importance for our primary purpose, which is to illustrate our computational approach.

[24]A. M. Karo and J. R. Hardy, Phys. Rev. 141, 696 (1966).

[25]G. Raunio, L. Almqvist, and R. Stedman, Phys. Rev. 178, 1496 (1969); J. R. D. Copley, R. W. MacPherson, and T. Timusk, *ibid.* 182, 965 (1969).

[26]J. E. Ralph and M. G. Townsend, J. Phys. C 3, 8 (1970).

[27]C. C. Klick, D. A. Patterson, and R. S. Knox, Phys. Rev. 133, A1717 (1964).

Thermal Conductivity and Specific Heat of Noncrystalline Solids*

R. C. Zeller† and R. O. Pohl

Laboratory of Atomic and Solid State Physics, Cornell University, Ithaca, New York 14850

(Received 28 May 1971)

The thermal conductivity of vitreous SiO_2, Se, and silica- and germania-based glasses has been measured between 0.05 and 100 °K. Comparison with earlier work on noncrystalline solids shows that they all have the same conductivity within a factor of 5 over the entire temperature range investigated, with the same characteristic plateau around 10 °K, and that their conductivity varies as T^n, $n \sim 1.8$, below $T = 1$ °K. Furthermore, the average phonon mean free path is large by comparison with the phonon wavelength, about 10^{-4} cm at 2 °K and decreasing as T^{-4} at larger T, suggesting a Rayleigh-type scattering mechanism. Such a mean free path can be quantitatively explained by approximating the glassy structure with that of a crystal in which every atom is displaced from its lattice site. Then every atom scatters like an interstitial atom, or—even simpler—like one that is missing at its regular lattice site, with a scattering cross section determined by the missing mass (isotopic defect). The specific heat of amorphous SiO_2, GeO_2, and Se has been found to vary as $AT + BT^3$ between 0.1 and 1 °K, with $A = 10$ erg/g °K^2 to within a factor of 2. This departure from the Debye specific heat may be characteristic of the glassy state, as all earlier measurements of other glasses [polystyrene, glycerol, Lucite (PMMA)] indicate a similar anomaly. Its origin is not clear. Impurities or surface effects through adsorbed gases are unlikely because of the many samples and experimental techniques used in different laboratories. We have tried to attribute the anomaly to low-lying electronic states, motional states of ions, trapped atoms or large groups of atoms, or one-dimensional vibrations within a three-dimensional solid, so far without success. At the present time, the only independent evidence for these excitations appears to be in the low-temperature thermal conductivity at $T < 1$ °K described above.

I. INTRODUCTION

The thermal conductivity of noncrystalline dielectric solids differs markedly from that of crystalline ones.[1,2] As an example, Fig. 1 shows the conductivities of crystalline and vitreous silicon dioxide. In crystals, the conductivity increases with decreasing temperature because the anharmonic umklapp processes become less frequent, and hence the phonon mean free path increases. Eventually, the mean free path becomes comparable to the sample dimensions, and the conductivity goes through a maximum and then decreases as the specific heat decreases.[3] The conductivity of crystals depends very much on the material, and in addition any disturbance of the lattice periodicity lowers the conductivity in a sometimes very characteristic way, as shown in Fig. 1, for example.[4] In noncrystalline solids, the conductivity is several orders of magnitude smaller than in crystals, it decreases monotonically with decreasing temperature, and furthermore it is independent of the chemical composition: In Fig. 2, the conductivity of vitreous silica[2,5-7] is compared with that of silica-based glasses containing large amounts of other oxides.[2,8-13] The conductivities are practically